

# Design and Evaluation of an Active Artificial Spine in a Hominid Robot

Daniel Kuehn, Alexander Dettmann,  
Frank Kirchner

German research center for artificial intelligence  
GmbH - Robotics Innovation Center (DFKI RIC)  
Bremen, Germany  
e-mail: Daniel.kuehn@dfki.de

Frank Kirchner

University of Bremen, Faculty of Mathematics and  
Computer Science  
Bremen, Germany

**Abstract**—With increasing mechanization of our daily lives, the expectations and demands in robotic systems increase in the general public and in scientists alike. Especially disaster scenarios shows that the robotic systems not only have to face a variety of different tasks during operation but also have to deal with different demands regarding the robot’s mobility characteristics. To be able to cope with future requirements, it seems necessary to develop kinematically complex systems that feature several operating modes. Often disregarded in robotics, yet extensively used in nature, are the degrees of freedom introduced by the spine. This paper presents the latest work on the hominid robot Charlie, whose morphology is oriented on chimpanzees and which has the possibility due to its electromechanical structure and the degrees of freedom to walk with different gaits in different postures. Besides its degrees of freedom in its limbs, the robot features an active artificial spine, equipped with sensors in the structure to allow a dual use; both as a structural part as well as a 6-DoF force/torque sensor. This paper analyses the benefits of an active spine experimentally. The results show, that the exploration of the range of motion is improved and that less requirements on joint velocities are lowered.

**Keywords;** Bio inspired robot, artificial spine, hominid, bipedal and quadrupedal locomotion

## I. INTRODUCTION

Nature makes extensive use of every Degree of Freedom (DoF) introduced by the spine. The spine’s role varies in different vertebrates, depending on their body shape, weight, and type of locomotion. In general, nature uses a spine as central element with several purposes like adding additional DoF, absorbing shocks, or storing and releasing energy to increase the overall walking efficiency. In a hunting cheetah, the spine is periodically bending and stretching and thus supports the galloping gait of the animal. In humans, in a bipedal stance the spine can support manipulation tasks to such an extent that the legs can remain stationary. These two examples illustrate that the support of motion patterns highly depends on the favored form of locomotion. The spine of a quadruped provides less flexibility for manipulation capabilities, but provides an ideal support for locomotion.

Introducing an active, artificial spine into a robotic system provides the potential to improve existing behaviors or gaits in terms of stability and energy efficiency. Furthermore, the possibility is given to realize new motion patterns with the robot. Though numerous research groups successfully developed robots that mimic the appearance and/or the locomotion patterns of their natural counterparts,

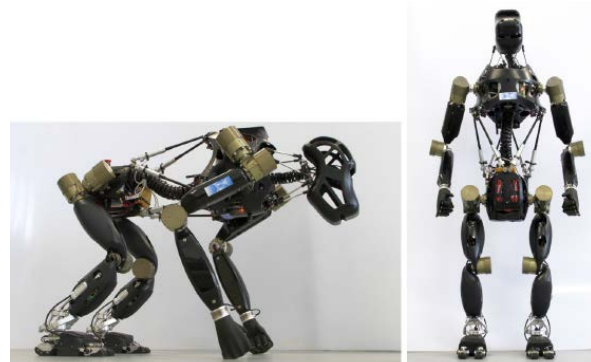


Figure 1: The updated version of the hominid robotic system Charlie

e.g., SpaceClimber [1], LS3 [2], Starleth [3], or LittleDog [4], the integration of an actively controlled spine is rarely investigated. As a consequence of these rigid connections, the motion of most robotic systems appears static and restricted. In humanoid robots, such as Atlas [5] or Reem-B [6], flexible body kinematics play a larger role. This is because the advantages and capabilities listed above come with the expense of increased mechanical and control complexity. Nevertheless, by looking at possible application areas, the benefits of dealing with this extra complexity become clear.

To increase a robots capability and to take advantage of the mentioned characteristics, some robotic research groups are introducing passive and active spine-like structure into their mobile robots. Santos et al. [7] presents an example for a walking and climbing robot equipped with an artificial passive spine. An active approach is pursued in [8], where the design of spine-like structures for multi-legged systems is described. Mizuuchi et al. [9] and Holland et al. [10] each introduced tendon-based approaches, by copying the design from natural spines and implemented it in adult sized humanoid robots. However, it has to be stated that the closer the artificial spines are designed after their natural counterpart, the more limited is the functionality. This is due to weight issues or the complex design and thus control difficulties.

Charlie [11] (see Fig. 1) is a hominid robot, which was developed to investigate quadrupedal and bipedal locomotion within one system. Due to the desired multi-functionality, the design was inspired by multi-talented animals such as the chimpanzee (*Pan troglodytes*). These animals regularly display quadrupedal and bipedal

locomotion, but are also capable of a variety of other behaviors including climbing and manipulation. For Charlie, multi-point-contact feet are essential to support bipedal locomotion. Despite the bipedalism ability, Charlie has to perform a posture transition, from a four-legged pose to a two-legged. For this purpose, it is essential to increase the robots general mobility. Although some of the mentioned multi-legged systems have one passive or active DoF in their body, structural enhancements were necessary in order to achieve a higher mobility and to allow alternative motion sequence. So, an active spine with six DoF was integrated.

In this paper, the utilization of an active spine for a quadrupedal locomotion in analyzed in order to see whether the advantages outweigh the high integration and control effort. The structure of the paper is as follows. At first, the electromechanical system design will be introduced with special focus on the robot's artificial spine. An overview over the control software is provided in Section III. Section IV describes the experiments performed and discusses the results. A conclusion and outlook is given in the final section.

## II. ARTIFICIAL SPINE

The dimensions of Charlie's limbs as well as its appearance are inspired by chimpanzees. Overall, Charlie features more than 330 sensor inputs and has 37 DoFs. The power consumption of the entire control electronics is about 48W. The focus of this chapter lies on the spine in a natural counterpart of Charlie. Detailed information regarding the design of the hominid robot with all its subsystems like actuators and multi-point contact feet can be found in [11].

In nature, a spine can usually be divided into three sections: the cervical, the thoracic, and the lumbar spine [12]. The thoracic and lumbar section are often merged and called thoracolumbar section. The Range of Motion (RoM) of the thoracolumbar spine section is displayed in Table I, since it is the most interesting part for a technical abstraction and implementation in a robotic system. The design of Charlie's spine follows the principle of a Stewart platform [13] and thus provides high stiffness with a possibility of light-weight design, which are excellent properties for the use as a body structure of a mobile robot. Charlie's front and rear body are connected via rods. The design of a 250mm long rod is shown in Fig. 2(c). In the middle of the spine a cable duct is installed, which is comparable to the natural spinal column, because of its main function of transmitting data between brain and body. Each rod has an one-dimensional force sensor integrated and due to the rod arrangement, only compression and tension forces can occur. The rod is connected via a lever on top to a brushless direct current motor and on the bottom with a hitch joint to the hip.

Table I: Range of motion of the thoracolumbar spine section in humans according to [12].

Degree of freedom	Range of motion (°)
Left/right rotation (torsion)	-35 to 35
Backward / forward flexion	-35 to 105
Lateral flexion	-40 to 40

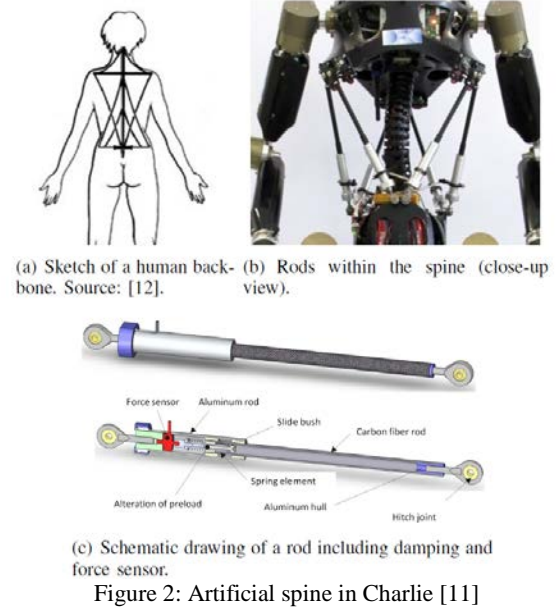


Figure 2: Artificial spine in Charlie [11]

In this technical realization, the lever arms are not applied to the spinal column like in nature, but they fulfill the same functionality. By comparing Fig. 2(a) with Fig. 2(b), the similarities between the spine in nature and the artificial one can be seen. The lever, connecting rod and motor, is 20mm long and defines the workspace of the spine. Overall, six motors are used to drive the spine. With Charlie's artificial spine, the maximum left/right rotation, i.e. the torsion, is from  $-28^\circ$  to  $28^\circ$ , the forward / backward flexion is from  $-18^\circ$  to  $18^\circ$ , and a maximum lateral flexion from  $-16^\circ$  to  $16^\circ$  is reached. The maximum translation on the x-axis is 44mm, allowing the robot to vary its body length by stretching or shortening itself. On the y-axis, a lateral translation between front and rear body of together 120mm is possible. On the z-axis, a shift of 108mm between front and rear body can be realized. By increasing the lever lengths, the spine's RoM is increased as well.

The power consumption for the installed electronics is measured, while the robot is suspended, i.e. no torques are needed for standing. Charlie's central electronics operates with 48V and consumes about 10.5W, whereas the spine electronic consumes 7W. An overview of the electronics and sensors installed in Charlie is given in Fig. 3, where the highly distributed control approach can be seen. The Motion Control Unit is the central node in Charlie. In this unit the motion control program is processed, the desired joint positions are generated and sent to the respective joints. The motion controller can treat the spine like a normal joint. The spine controller receives the desired translation and rotation values and then calculates the required angular positions of the respective motors.

The spine control electronics, which can control all six motors at the same time, is custom made and was developed to enable an efficient control of the spinal column structure. This PCB consists of three stacked boards. The upper and lower boards have three motor driver stages each and the middle one is equipped with a Spartan6 FPGA, as well as

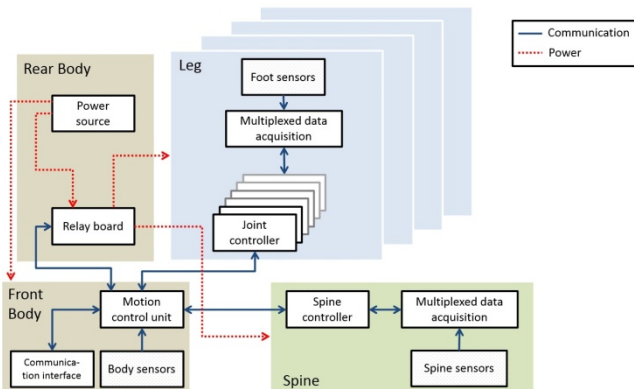


Figure 3: Block diagram of the electronic components and sensors within the system [16]

memory and communication modules. The individual boards are stacked, allowing the FPGA to control all motors. In addition to all motor sensors (phase, Hall sensors and encoders), the boards also have additional options for reading out six iC-house sensors, which are applied on the levers and provide the absolute position of each motor.

Currently, the lever is 20mm long and defines the workspace of the spine. By changing the lever length, the workspace of the spine changes as well. It has to be mentioned that the range of motion listed above cannot be reached simultaneously. This becomes clearer when looking at the possible workspace as depicted in Fig. 4.

The figure shows the possible movement of the rear body relative to the front body in  $x$ ,  $y$  and  $z$  direction. The respective movement range is indicated within the figure as well. The values indicate the maximum movement within the robot's body coordinate systems.

For example, if the desired translation for  $y = 0$  and  $z = 0$ , the movement range on the  $x$  axis is between 0 and 42mm (see first plot in Fig. 4). If, on the other hand, a translation on the  $z$ -axis to its maximum and a rotation on the same axis is desired, the desired position cannot be reached. Both movements to the extrema at the same time are mutually exclusive, since a rotation around this axis requires a modification of the translational position.

### III. BEHAVIOR-BASED MOTION CONTROL

The reactive motion control is based on a behavior-based architecture realized in BAGEL [14]. It follows an hierarchical modular concept consisting of general-applicable and robot-specific behavior modules, where every module can contain further submodules to reduce module complexity and to increase module reusability. On the highest control layer, a Central Pattern Generator (CPG) is used to derive a gait-dependent step cycle for every limb.

This signal is sent to every leg or arm controller in which a state pattern generator is triggered to derive a foot trajectory. In addition, the progress of the step cycle is sent to a body controller behavior, which generates a gait dependent body trajectory to maintain a body position over the ideal Center

of Support Polygon (CoSP). Both, the open-loop generated foot positions and the body trajectory are influenced by reactive behaviors to adapt to unstructured terrain or unforeseen situations.

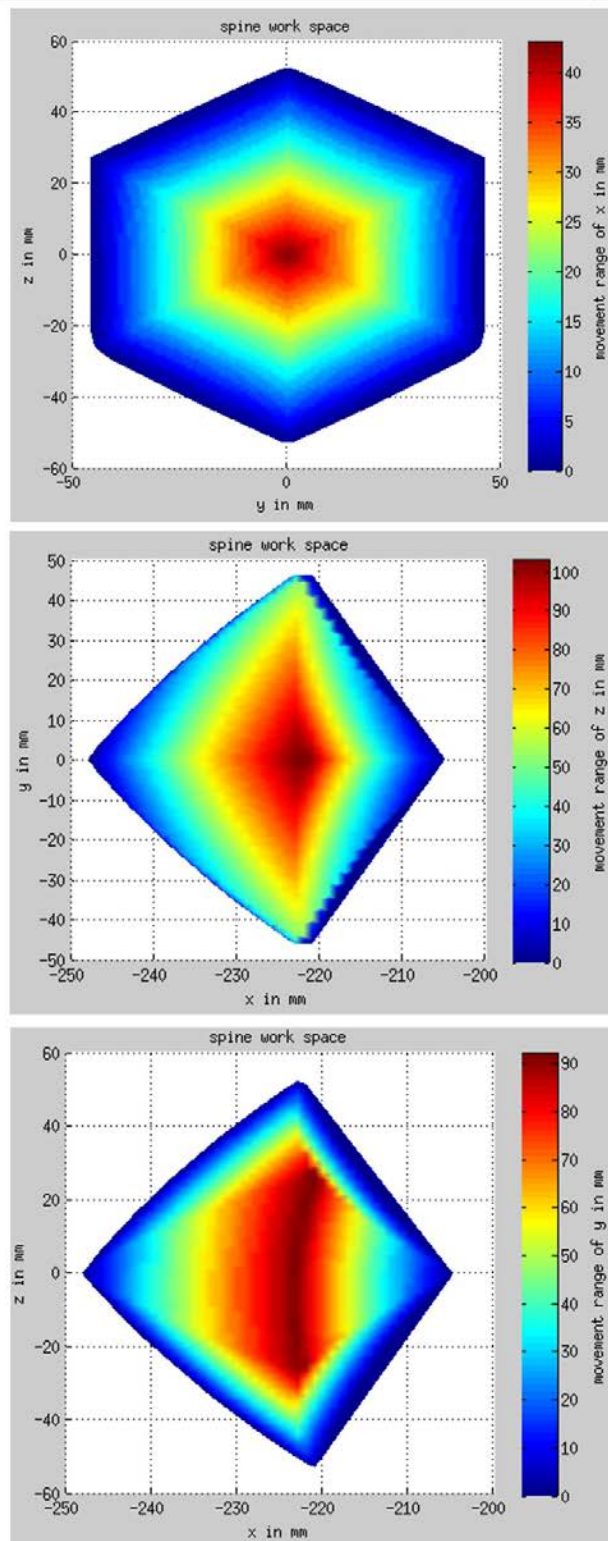


Figure 4: The range of motion of the spine structure

All posture and locomotion parameters are defined in an ideal frame which is parallel to the ground, so called locomotion frame (*LocoFrame*). The generated foot positions are transformed from *LocoFrame* to the robot coordinate system (*RobotFrame*) which is fixed to the robot. With the help of the body forward kinematics, a target position for each foot in its limb coordinate system (*LimbBase\*Frame*) is calculated. Finally, inverse kinematics are used to compute the joint targets.

After giving a brief overview over the basic behavior modules, the spine support behavior module is introduced which utilize Charlie's unique body morphology to support locomotion

### A. Central Pattern Generator

The CPG module generates an internal clock, which triggers different phases of a walking cycle. It consists of a period generator, a period coordinator, and a gait generator. The period generator generates the internal robot clock, a periodic saw curve normalized between zero and one. The time step increment ( $t_{step}$ ) depends on the desired step cycle time ( $t_{cycle}$ ) and the update rate of the control ( $t_{period}$ ) (1).

$$t_{step} = \frac{t_{period}}{t_{cycle}} \quad (1)$$

The period coordinator starts and stops the internal clock depending whether a movement is desired or not. When no movement is desired, the period progress continuous until all legs are placed on the ground. Then, the period counter is set back to the point where no movement is desired. So, the legs which were not allowed to move anymore will be the first to start again if new movement is desired. The gait generator defines at what time each leg starts with its movement. It supports walking gaits for two-legged and four-legged walking. The parameter *phase shift* can be set to influence the time between consecutive legs. A full phase shift will evenly distribute the start of each leg movement, whereas no phase shift will lead to a cross gait for quadrupedal walking.

### B. Limb Controller

The basic stance is defined by the  $step\_base\_x,y$  parameter and an additional  $arm\_offset\_y$  to define foot positions well suited for both, leg and arm kinematics (Fig. 5). It is also possible to set an individual offset for each limb. In general, all parameters can be changed during runtime, but these are actually set when the corresponding leg is in the air to avoid huge shear forces. A desired translation or rotation between both frames can be achieved by setting a desired  $body\_shift\_x,y,z$  or  $body\_rot\_roll\_pitch\_yaw$ , respectively. The Cartesian foot trajectory is based on the current progress of the step cycle which consists of a stance ( $t_{stance}$ ) and a swing phase ( $t_{swing}$ ). The latter is divided into a lift ( $t_{lift}$ ), shift ( $t_{shift}$ ), and down phase ( $t_{down}$ ), each defined by a portion of the overall step cycle (2). In order to realize a statically stable walking pattern, their sum, i.e. the swing time, must not exceed a maximum leg time, defined by the gait.

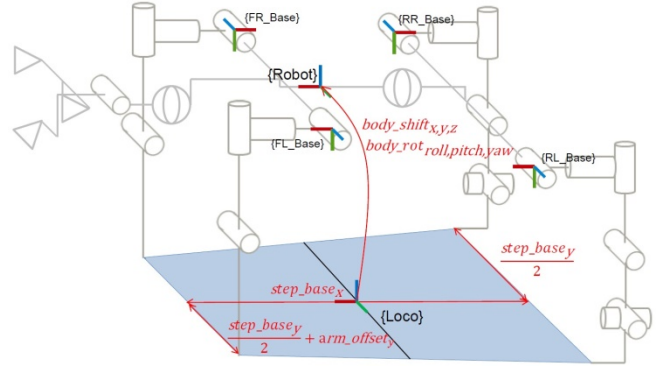


Figure 5: Charlie's kinematics, frames and parameters to define the posture

$$1 = t_{stance} + t_{swing} = t_{swing} + t_{lift} + t_{shift} + t_{down} \quad (2)$$

A leg can only enter the lift phase when movement is desired. During stance, a leg is moved on the ground with a speed defined by the length of each step in longitudinal and lateral direction ( $step\_length_{x,y}$ ) and the step cycle time. Thus, (3) is defining the overall robot speed.

$$v_{xy} = \frac{step\_length_{xy}}{t_{cycle}} \quad (3)$$

In addition, this open-loop trajectory generation is adapted by an elevation and depression reflex to cope with unstructured terrain. This is done in two ways. First, a leg is crouched when contact was detected during down phase, i.e., the z-position of the foot shall stay constant, so a compensating offset is generated which superposes the normal walking trajectory. Second, a leg is stretched when no contact is established during stance phase.

### C. Body Controller

This behavior module shifts the body over the ideal CoSP in order to maintain a stable walking posture. With the knowledge of the gait, it knows which legs to use for computing the CoSP (4).

$$CoSP = \frac{\sum_{e=1}^E foot\_pos_e}{E} \quad (4)$$

, where E is the number of legs in stance phase and  $foot\_pos_e$  their desired position in *Loco Frame*.

A spline interpolator is used to generate a curve for every swing time of a leg, having its mid target over the CoSP and the target in the middle of the current and consecutive CoSP. For the target point, a target speed is estimated to avoid a start-stop behavior during leg transition. Thus, for four-legged walking, an eight-shaped trajectory is generated. To prevent tipping over, the Zero Moment Point (ZMP) [15] is continuously measured, transformed into *LocoFrame*. While walking on plane ground, one will see that the ZMP will follow the desired body trajectory. As soon as the robot

climbs obstacles or enters a slope, the body will tilt with respect to gravity and the projection along the gravity vector will cause a difference between ZMP and desired body position. Then, a balance controller will compensate this difference, thus avoiding a crossing of the ZMP over one edge of the support polygon.

Besides, the position difference, differences in speed and acceleration are also taken into consideration to form a precise and fast control loop. First, a desired acceleration  $acc_{des}$  is computed based on (5).

$$acc_{des} = k_{pos} \cdot diff_{pos} + k_{vel} \cdot diff_{vel} + k_{acc} \cdot diff_{acc} \quad (5)$$

, where  $k^*$  are the control gains and  $diff^*$  the differences between desired and measured position, speed, and acceleration, respectively. With this, the future desired position ( $pos_{des}$ ) is calculated (6) and used to set  $body\_shift_{x,y}$ .

$$pos_{des} = pos_{des} + vel_{des} \cdot t_{step} + acc_{des} \cdot t_{step}^2 \quad (6)$$

Additionally, the next desired velocity ( $vel_{des}$ ) is calculated for the next processing cycle (7).

$$vel_{des} = vel_{des} + acc_{des} \cdot t_{step} \quad (7)$$

#### D. Spine Support

In Charlie, the movement of the actuated artificial spine supports all different kinds of motions including the locomotion. To be more specific, by setting the desired step length to a value within the overall range of motion of the spine, e.g., to 20mm per cycle and using the highest scaling factor  $spine\_k$ , the leg joints will hold their position and a forward motion including the lift-off and touchdown events of each foot is realized only through the movement of the spine. This means, its rotational and translational movement have an influence on the position and orientation of the front and rear feet (schematically shown in Fig. 6). Therefore, the trajectories of the limb's endpoints have to be adapted accordingly.

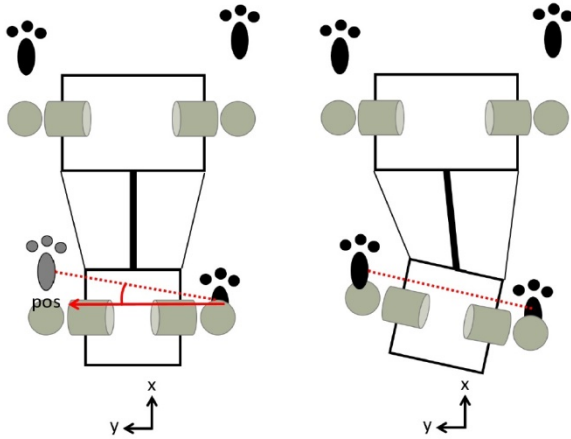


Figure 6: Schematic drawing of the spine motion while walking. Left: Actual and desired position of the RL leg ( $pos$  and the greyed out foot, respectively). Right: Movement of the hip with respect to the shoulder to reach the desired foot position [16].

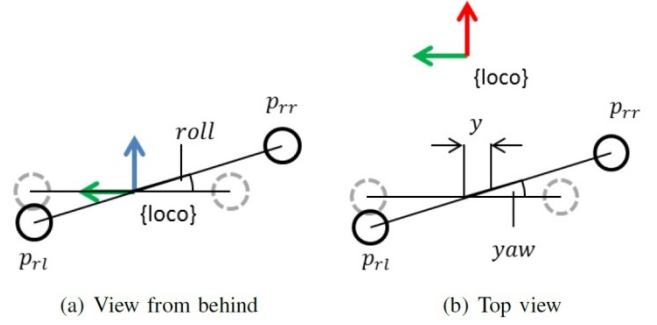


Figure 7: Spine support inputs and outputs (the dashed grey circles mark the default posture without movement and offsets)

This is done by the spine support behavior module. This module uses some degrees of freedom of the spine to reduce the needed range of motion of the rear legs during walking (Fig. 7). The spine is translated along the  $y$ -direction, if both rear legs are shifted to the same side (8).

$$spine_y = \frac{y_{rl} - y_{rr}}{2} \quad (8)$$

The spine is rotated around the  $z$ -axis to compensate a difference in  $x$ -direction (9).

$$spine_{yaw} = atan2(x_{rl} - x_{rr}, y_{rl} - y_{rr}) \quad (9)$$

The spine is rotated around the  $x$ -axis to compensate a difference in  $z$ -direction (10).

$$spine_{roll} = -atan2(z_{rl} - z_{rr}, y_{rl} - y_{rr}) \quad (10)$$

All compensation movements can be scaled by a factor  $spine\_k$ , since the spines's limited RoM cannot cover all possible foot differences.

## IV. EXPERIMENTAL EVALUATION

As described in Section III, Charlie's control is based on several behavior producing modules which all contribute to the overall locomotion behavior. Due to the hierarchical structure, a set of basic behavior modules can be used to generate locomotion patterns for every type of four-legged system. In addition, the spine support behavior module modulates the default trajectory by utilizing the special kinematical structure of Charlie. Here, the benefit of this module concerning the range of motion and velocities of the first hip and knee joint is investigated, since they contribute most to the forward motion. As reference, the same pattern but without active support of the spine is used, i.e., the spine motors are still actively holding the initial position.

### A. Range of Motion Analysis

First, a walking pattern of moderate speed (60 mm per sec) was created and compared with and without spine support. When taking a look on the required joint angles and velocities during walking (Fig. 8), one notices that the

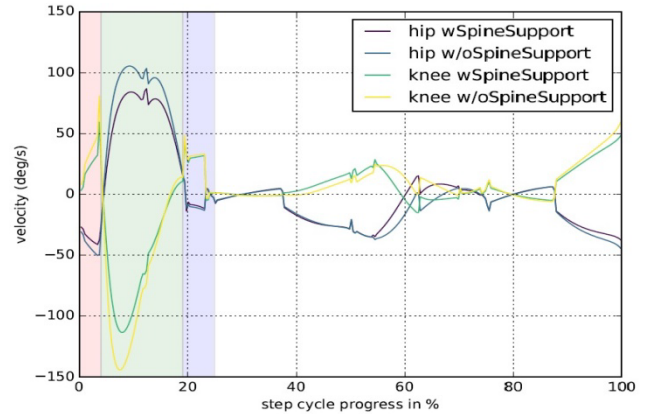
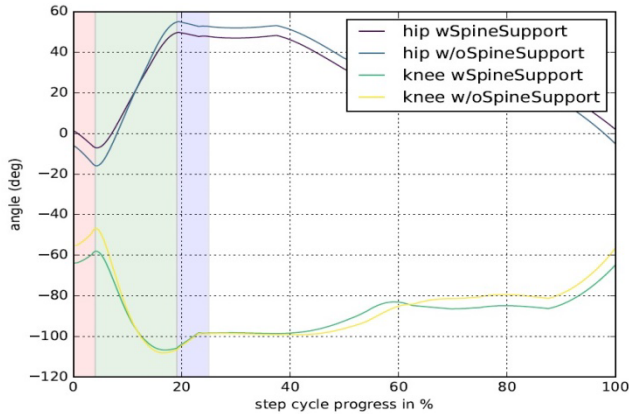


Figure 8: Required joint angles and velocities during walking at constant speed with and without utilization of the spine. Lift shift and down phase is colored with red, green, and blue background, respectively. Left: hip joint angle. Right: knee joint angle

demands on movement range and velocity are reduced, when walking is supported by the spine. The yaw rotation of the spine reduces the distance of desired foot position towards the  $LimbBase * Frame$ . Thus, especially in the phase around liftoff (from 85% up to 10%), the knee is less stretched which has three advantages.

First, more movement range of the leg remains, which is crucial when reactive behaviors want to modulate the desired foot position, e.g., stretching the leg further when the foot steps into a hole. Second, in this posture, the step  $length_x$  can be increased from 390mm to 420mm when utilizing the spine until a leg loses ground contact before the actual lift phase starts. In general, the workspace of an limb is increased, highly depending on the position of the end effector within 6% to 16%.

Third, as also shown in Fig 8(b), the spine motion supports the walking by reducing the maximum joint speed requirements to generate a forward motion. A reduction of the maximum speed has further electro-mechanical advantages. Lower accelerations entail less mechanical stress especially to the gear. In addition, this leads to lower power requirements on the three motor phases. Both factors will have a positive effect on reliability and maximum lifetime of the actuator including its control PCB. For locomotion, this can result in an increase of both, walking speed and stability. Less dynamics are inserted into Charlie and the robot is capable of moving faster, since the same cycle time allows larger steps.

### B. Walking ground

To allow a comprehensive, scientific evaluation of the developed robot Charlie, the system is tested in different environments like solid grounds, indoor or on a garden path, as well as on loose soil like a gravel field.

Terrain gravel defines gravel with varying dimensions from 1.5 cm x 1.5 cm x 2.5 cm to 3 cm x 3.5 cm x 4.5 cm.

Table II shows the average power consumption while walking on terrain lab and terrain gravel with speed setting medium in varying setups, the energy efficiency is specified as required Watt per meter. The lower the value the more energy efficient is the walking. The distance covered for this speed setting is 30 cm per step cycle. The cycle step time is set to 5 sec. It can be seen for both setups that if the robot is walking on even ground, like a laboratory floor, the overall current consumption is remains the same, despite the movement of the six actuators in the spine. This can be explained with the reduced movement of the legs, when the spine is active.

Table II: Power consumption while walking on terrain lab and terrain gravel with speed setting medium and varying setups. The value is the mean value of one complete step cycle.

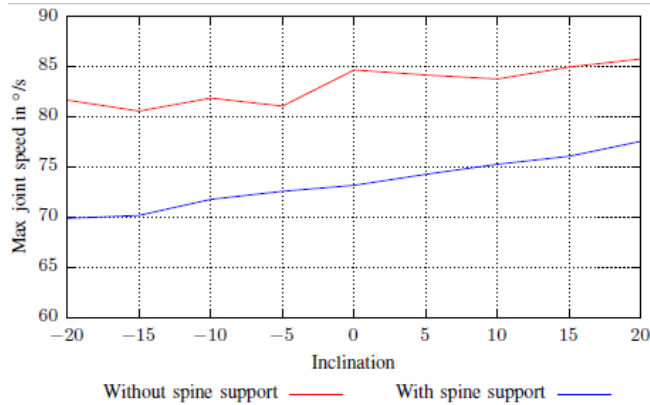
Setup / Energy efficiency	Without spine motion in [W per m]	With spine motion in [W per m]
Terrain lab	118.3	118.3
Terrain gravel	133.3	137.3

### C. The Active Spine and its Influence During Slope Climbing

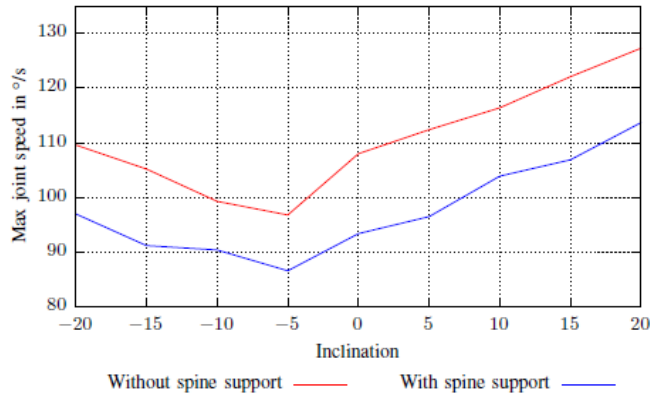
For this experiment, an infinitely variable, indoor ramp with a wooden surface is used. The incline is increased in 5° steps and ranges from -20° to 20°. A positive degree indicates an uphill walking of the robot and a negative degree stands for downhill walking. The walking speed was set to a low speed of 30 mm per sec allowing the robot to overcome all inclinations without any changes in the motion control. Each run on each inclination is repeated at least three times. A run is considered as complete, if the robot has performed at least 10 full walking cycles. One walking cycle is complete, if all four legs are moved.

The data shown in the following figures and tables are the mean values over three runs. No safety harness or alike are used during the experiments, to obtain authentic and undistorted results. While performing the experiments, no parameter aside from the respective inclination and the selection of the desired setup has been modified by the operator.

As shown in Fig. 9, the active spine support reduces the maximum joint velocities in all inclines. The joint speed changes in different inclines due to the posture adaption of the stability controller. For both joints a reduction between  $10^\circ$  per sec to  $15^\circ$  per sec is recorded, which corresponds to a decrease of up to 14%. The overall power consumption, however, remains nearly constant for all setups. The spine motors need additional power for driving, however, energy is saved by the legs due to lower accelerations.



(a) RR hip joint 1



(b) RR knee joint

Figure 9: Maximum joint speeds in the rear right leg in different inclinations

Table III: Pulling forces of are applied on the spine. The standard deviation is indicated in parentheses.

Axis / Applied load (N)	x-axis (N)	y-axis (N)	z-axis (N)
47.1	42.2 (1.3)	45.9 (2.4)	45.2 (2.2)
94.7	89.3 (1.5)	91.5 (2.4)	86.8 (1.1)
142.2	132.4 (3.0)	132.3 (2.4)	134.0 (1.3)

#### D. Validation of the Spine as a Six-DoF Force/Torque Sensor

As mentioned above, most robots have a rigid body with attached legs. Charlie's artificial spine consists of six rods, which interlink the front and rear body. In each rod, an one DoF force sensor is integrated. All six sensors can be combined into a virtual six DoF force/torque sensor, which is able to measure the forces and torques between hip and shoulder. To validate the functionality of this combined sensor, different experiments are performed. Due to limited space only one experiment is shown.

Pulling forces of about 5 kg, 10 kg, and 15 kg are applied to the spine via weight plates and a wire rope hoist. Charlie is hovering over the ground in a quadrupedal posture. The pulling force is applied in all three directions, so one after the other each force pulls on the hip downwards, sideways or to the back. The weight plates are applied to the spine via a wire. The data is shown in Table III.

As for the first experiment, all actuators are switched on to hold the position. It has to be noted that the weight plates actual weight differs from the advertised weight, thus the plates are lighter than specified. The difference depends on the individual weight plates and is not the same for each plate. For the 5 kg plate, the actual weight differs about 200 g, for the 10 kg plate about 350 g, and for the 15 kg plate the difference is 500 g. As it can be seen in the Table III, the measured values are close to the expected ones. The differences between the three axes can be caused of minor differences in the lengths between the individual rods. In addition, sensor accuracy as well as the experimental setup with friction between wire and test rack are possible reasons.

#### E. Measured Forces and Torques in the Spine While Walking

The data shown in the following tables are the mean values following the same experiment pattern as described in Section IV-C. The columns in Table IV list the mean value of forces and torque acting on the spines x-, y-, and z-axis while walking on even ground. The upper part of the table shows the data for the force measurement and the lower part shows the data for the torque measurement.

It can be seen that the walking speed has no direct influence on the forces acting on the spine. The acting force is slightly increased in setups with active spine motion, due to the movement of the spine.

Table IV: Measured spine forces and torque while walking with 90mm per second on even ground. The standard deviation is indicated in parentheses.

Force	x-axis (N)	y-axis (N)	z-axis (N)
w/o spine support	4.3 ( $\pm$ 3.2)	7.5 ( $\pm$ 3.3)	-26.5 ( $\pm$ 3.3)
w spine support	6.4 ( $\pm$ 3.0)	9.4 ( $\pm$ 3.1)	-24.6 ( $\pm$ 2.9)
Torque	x-axis (Nm)	y-axis (Nm)	z-axis (Nm)
w/o Spine Support	12.4 ( $\pm$ 3.5)	8.3 ( $\pm$ 3.5)	-20.4 ( $\pm$ 3.4)
w spine support	9.3 ( $\pm$ 3.4)	5.9 ( $\pm$ 3.3)	-20.0 ( $\pm$ 3.2)

However, the data indicate that the control software and thus the walking pattern and kinematic calculation are well realized by the joints, since nearly no pushing or pulling forces can be measured. In addition, the measured torques while walking with different setups are shown. In contrast to the forces, one can see that the acting torques are reduced when the spine motion is active. This allows the conclusion that an active spine movement can help to reduce possible tension between front and rear body.

Due to the multitude of installed sensors within the presented robot, the implementation and study of a holistic force-based robot control is now possible. The torques that are applied by the rear legs to the body can be perceived within the spine and due to its motion capabilities, the flow of forces can be supported and transferred to the front legs, to gain a fast and energy-efficient walking pattern.

## V. CONCLUSION AND OUTLOOK

The paper presents the design of the artificial spine, which follows the principle of a Stewart platform, and focuses on its actuation and its sensory equipment. In addition, a behavior that utilizes an active spine during quadrupedal locomotion is introduced. It is shown that when the spine is supporting the locomotion, the robot's RoM is increased of up to 16%. While walking the spine motion helps to reduce the maximum joint velocity requirements to generate a forward motion. A reduction of the maximum speed has several electromechanical advantages. Lower accelerations entail less mechanical stress to the motor and the gear, as well as lower power requirements on the three motor phases. Both have a positive effect on reliability and lifetime of the actuator including its local electronics. For walking, this can result in an increase of walking speed of the robot, since the same cycle time allows larger steps.

Furthermore, due to the installed force sensors in the rods, the spine can be used as a six-axes force/torque sensor. The functionality of this virtual force/torque sensor is experimentally validated. These sensors allow in future the implementation and study of a holistic force-based robot control, introducing a flow of forces introduced by the rear legs, not only transferred but actively supported by the artificial spine to the front legs, allowing to realize a fast and energy-efficient walking pattern.

## ACKNOWLEDGMENT

The presented work was carried out in the project VIPE funded by the German Space Agency (DLR, Grant numbers: 50NA1516) with federal funds of the Federal Ministry of

Economics and Technology (BMW) in accordance with the parliamentary resolution of the German Parliament.

## REFERENCES

- [1] S. Bartsch, T. Birnschein, M. Römmermann, J. Hilljegerdes, D. Kuehn, and F. Kirchner, "Development of the six-legged walking and climbing robot spaceclimber," *Journal of Field Robotics*, vol. 29, 2012.
- [2] D. Wooden, M. Malchano, K. Blankespoor, A. Howardy, A. Rizzi, and M. Raibert, "Autonomous navigation for bigdog," in *Robotics and Automation (ICRA)*, 2010 IEEE International Conference on, 2010, pp. 4736–4741.
- [3] M. Hutter, C. Gehring, M. Bloesch, M. A. Hoepflinger, C. D. Remy, and R. Siegwart, "Starleth: A compliant quadrupedal robot for fast, efficient, and versatile locomotion," in *Climbing and Walking Robots (CLAWAR)*, 2012.
- [4] M. P. Murphy, A. Saunders, C. Moreira, A. A. Rizzi, and M. Raibert, "The littledog robot," *The International Journal of Robotics Research*, vol. 30, no. 2, pp. 145–149, 2011. [Online]. Available: <http://ijr.sagepub.com/content/30/2/145.abstract>
- [5] M. Fallon, S. Kuindersma, S. Karumanchi, M. Antone, T. Schneider, H. Dai, C. P. D'Arpino, R. Deits, M. DiCicco, D. Fourie, T. Koolen, P. Marion, M. Posa, A. Valenzuela, K. Yu, J. Shah, K. Iagnemma, R. Tedrake, and S. Teller., "An architecture for online affordancebased perception and whole-body planning," MIT CSAIL, Tech. Rep., 2014.
- [6] R. Tellez, F. Ferro, S. Garcia, E. Gomez, E. Jorge, D. Mora, D. Pinyol, J. Oliver, O. Torres, J. Velazquez, and D. Faconti, "Reem-b: An autonomous lightweight human-size humanoid robot," in *8th IEEE/RSJ International Conference on Humanoid Robots*, Dec 2008, pp. 462–468.
- [7] D. Santos, B. Heyneman, S. Kim, N. Esparza, and M. R. Cutkosky, "Gecko-inspired climbing behaviors on vertical and overhanging surfaces," in *Proceedings of the IEEE International Conference on Robotics and Automation (ICRA)*, 2008.
- [8] K. Tsujita and K. Miki, "A study on trunk stiffness and gait stability in quadrupedal locomotion using musculoskeletal robot," in *Proceedings of the IEEE International Conference on Advanced Robotics*, 2011.
- [9] I. Mizuuchi, R. Tajima, T. Yoshikai, D. Sato, K. Nagashima, M. Inaba, Y. Kuniyoshi, and H. Inoue, "The design and control of the flexible spine of a fully tendon-driven humanoid kenta," in *Intelligent Robots and Systems, 2002. IEEE/RSJ International Conference on*, vol. 3, 2002, pp. 2527 – 2532 vol.3.
- [10] O. Holland and R. Knight, "The anthropomorphic principle," in *Proceedings of the AISB06 Symposium on Biologically Inspired Robotics*, 2006.
- [11] D. Kuehn, M. Schilling, T. Stark, M. Zenzes, and F. Kirchner, "System design and field testing of the hominid robot charlie," *Journal of Field Robotics*, 07 2016.
- [12] I. A. Kapandji, *Funktionelle Anatomie der Gelenke - Schematisierte und kommentierte Zeichnungen zur menschlichen Biomechanik Band III: Wirbels'aule*, 3rd ed. Hippokrates Verlag, Stuttgart, 1999.
- [13] D. Stewart, "A platform with six degrees of freedom," *Proceedings of the institution of mechanical engineers*, vol. 180, no. 1, pp. 371–386, 1965.
- [14] M. Langosz, L. Quack, A. Dettmann, S. Bartsch, and F. Kirchner, "A behavior-based library for locomotion control of kinematically complex robots," *Int. Conf. on Climbing and Walking Robots*, 2013.
- [15] M. Vukobratovic and B. Borovac, "Zero-moment point - thirty five years of its life." *I. J. Humanoid Robotics*, vol. 1, no. 1, pp. 157–173, 2004.
- [16] D. Kuehn, Design and development of a hominid robot with local control in its adaptable feet to enhance locomotion capabilities. 2016, Dissertation